

Impact of the Composition of Alcohol/Water Dispersion on the Proton Transport and Morphology of Cast Perfluorinated Sulfonic Acid Ionomer Thin Films

Xiao Gao, Kentaro Yamamoto,* Tomoyasu Hirai, Noboru Ohta, Tomoki Uchiyama, Toshiki Watanabe, Hideto Imai, Seiho Sugawara, Kazuhiko Shinohara, and Yoshiharu Uchimoto



Cite This: *ACS Omega* 2021, 6, 14130–14137



Read Online

ACCESS |



Metrics & More

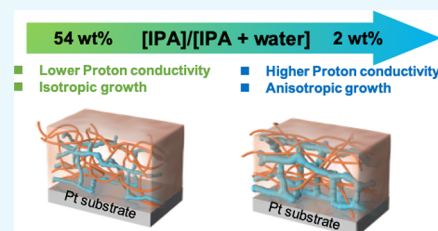


Article Recommendations



Supporting Information

ABSTRACT: The dispersion of perfluorinated sulfonic acid ionomers in catalyst inks is an important factor that controls the performance of catalyst layers in membrane electrode assemblies of polymer electrolyte fuel cells. Herein, the effects of water/alcohol compositions on the morphological properties and proton transport are examined by grazing incidence small-angle X-ray scattering, grazing incidence wide-angle X-ray scattering, and electrochemical impedance spectroscopy. The thin films cast by a high water/alcohol ratio Nafion dispersion have high proton conductivity and well-defined hydrophilic/hydrophobic phase separation, which indicates that the proton conductivity and morphology of the Nafion thin films are strongly influenced by the state of dispersion. This finding is expected to further understand the morphology and proton transport properties of Nafion thin films with different water/alcohol ratios, which has implications for the performance of the Pt/Nafion interface.



INTRODUCTION

Polymer electrolyte fuel cells (PEFCs) have received considerable attention owing to their high efficiency, high power density, and zero emission as fuel cell vehicles to microelectronics.^{1–4} In PEFCs, carbon-supported platinum (Pt/C) covered by proton-conductive perfluorosulfonated ionomers is the reaction field of the oxygen reduction reaction. Nafion is the most well-known proton-conductive material owing to its high proton conductivity, thermal stability, and mechanical properties.^{5–9} Nafion consists of a hydrophobic polytetrafluoroethylene backbone ($-\text{CF}_2-$) with perfluorinated chains on either side that terminate in hydrophilic sulfonic acid groups ($-\text{SO}_3\text{H}$).^{10,11} Under highly hydrated conditions, the hydrophilic groups form an ionic domain that is related to proton transport, whereas the hydrophobic backbone aggregates to provide high mechanical stability.^{8,9,12} The electrochemical properties, such as proton conductivity, of Nafion thin films on the catalyst are different from those of freestanding Nafion membranes.^{13–16} This is because the confinement effect significantly influences the domain orientations and anisotropy in Nafion thin films, as the ionomer thickness approaches the domain size of the copolymers.^{17,18} Thus, it is crucial to understand the relationship between the morphology and electrochemical properties of Nafion thin films on a catalyst.

In the fabrication of a membrane electrode assembly, the Pt/C catalyst is cast on Nafion membranes using a catalyst ink of a mixture of Nafion dispersion and the Pt/C catalyst. It has been reported that the molecular structure and properties of Nafion in the dispersion are influenced by the solvents.^{19–26} In high

dielectric constant solvents such as water, Nafion has a tightly packed structure with a sulfonic group on the outside and the perfluorocarbon backbone inside the molecule.^{19,21,22,27} In a low dielectric constant solvent such as isopropyl alcohol (IPA), Nafion has a loosely packed structure with the perfluorocarbon backbone on the outside and the sulfonic group on the inside of the molecules.^{27,28} In a mixed solution between water and IPA, the molecular structure of Nafion changes from a tightly packed structure to a loosely packed structure as the [IPA]/[IPA + water] ratio increases.²⁸ These molecular structures of Nafion influence the electrode performance of the PEFCs.^{25,26,28,29} These solvent effects can also change the interaction driving the ionomer–particle aggregation in an ink because inks with different water/alcohol ratios exhibit different aggregate sizes.^{30–32} Ngo *et al.*, via transmission electron microscopy, revealed that the aggregate particle size of Nafion molecules decreases as the IPA concentration increases from 20 to 80 wt % of IPA/water solvents.²⁸ A similar tendency was also observed by Berlinger *et al.*, who revealed that the aggregate size of the Nafion molecules increases as the water concentration increases.³³ Although several studies have attempted to understand the molecular structure of Nafion in

Received: February 2, 2021

Accepted: May 13, 2021

Published: May 25, 2021



ACS Publications

dispersions with different solvents or different IPA/water ratios, these studies have focused on Nafion in the dispersed state and not the Nafion film. To date, the relationship between the morphology and proton transport properties of Pt-supported Nafion thin film cast by Nafion dispersion with different IPA/water ratios has not been clearly understood.

To analyze the morphology of a Nafion thin-film catalyst, grazing incidence small-angle X-ray scattering (GISAXS) and grazing incidence wide-angle X-ray scattering (GIWAXS) are powerful tools.^{17,34–37} Our group has identified the quantitative relationship between the morphology and proton transport properties of Nafion thin films with different thicknesses after annealing treatment on a Pt substrate using these techniques combined with Pt-deposited interdigitated array electrodes.³⁸ It has been proved that the annealing treatment has impact on formation of hydrophilic and hydrophobic domains and the morphology change temperature depends on the film thickness. GISAXS/GIWAXS are useful for understanding the relationship between the morphology and proton conductivity of Nafion thin films cast on a Pt electrode using Nafion dispersions with different water/alcohol ratios.

In this study, we examine the correlation between the morphology and proton transport behavior of spun-cast Nafion thin films with different IPA/water fractions. Nafion films of 50 and 110 nm thicknesses on a Pt substrate cast by Nafion dispersion with different water/alcohol ratios are systematically investigated via GISAXS/GIWAXS and electrochemical impedance spectroscopy (EIS) methods in terms of morphological properties and proton transport behavior.

RESULTS AND DISCUSSION

The thicknesses of the as-prepared Nafion thin films were 50 and 110 nm, which were characterized by ellipsometry combined with the Cauchy model fitting as previously reported.³⁸ Figure 1 displays the proton conductivity of the

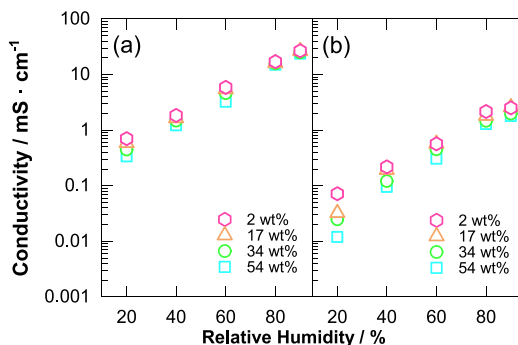


Figure 1. Proton conductivity of Nafion thin films with different thicknesses: (a) 110 nm and (b) 50 nm, cast using different IPA fractions of Nafion dispersion. Electrochemical impedance was conducted under a wide range of humidity from 20–90% RH at 25 °C.

cast Nafion thin films with different IPA fractions in the solvent and thicknesses (Figure 1a, 110 nm; Figure 1b, 50 nm) at 25 °C under 20–90% RH. The Nyquist plot is displayed in Figure S1, Supporting Information. In the case of the 110 nm film displayed in Figure 1a, the proton conductivity increased as the relative humidity increased in the range of 20–90% RH, for all samples, which exhibited humidity dependence as in a previous work.¹³ Moreover, the proton conductivity increased with decreasing IPA fraction in the cast solution. Comparing

the proton conductivity of the Nafion thin films cast by dispersion with IPA fractions of 54 and 2 wt %, the gap became larger at lower RT (Figure 1a and Figure S2a), and the gap at 20% RH indicated the greatest difference (54 wt %: 0.33 mS/cm; 2 wt %: 0.70 mS/cm). A similar tendency was observed for 50 nm (Figure 1b and Figure S2b). These results indicate that the proton conductivity of the Pt-supported Nafion thin films is influenced by the IPA fraction in the cast solution. In particular, the difference in proton conductivity between 2 and 54 wt % IPA cast thin films increased as the thickness decreased to 50 nm. It can be noticed that the difference in proton conductivity between 2 and 54 wt % IPA cast thin films at low %RH is larger in a 50 nm-thick film than a 110 nm-thick film. The reason for that will be discussed in detail later.

The morphologies of the as-prepared Nafion thin films cast by dispersion with different IPA fractions were examined by GISAXS and GIWAXS measurements. Figure 2 displays the GISAXS 2D patterns of Nafion thin films with thicknesses of 50 and 110 nm, cast by different IPA fractions of Nafion dispersion. The scattering patterns are plotted as scattering vector q in 2D, and the measured intensity is reported as a function of the magnitude of the scattering vector.³⁹

$$q = \begin{pmatrix} q_x \\ q_y \\ q_z \end{pmatrix} = \frac{2\pi}{\lambda} \begin{pmatrix} \cos 2\Theta \cos \alpha_f - \cos \alpha_i \\ \sin 2\Theta \cos \alpha_f \\ \sin \alpha_i + \cos \alpha_f \end{pmatrix} \quad (1)$$

α_i means the incidence angle; α_f and Θ mean the exit angles along the out-of-plane and in-plane directions, respectively. λ is the wavelength of the incident X-ray. In the case of the 110 nm-thick Nafion thin films cast by dispersion with 54 wt % IPA fraction, the scattering ring appeared near $q = 1–2 \text{ nm}^{-1}$. The scattering ring is called the “ionomer peak”, which arises from the ordered structure of the hydrophilic ionic domain in Nafion thin films.^{40,41} As the IPA fraction decreased to 2 wt %, the ionomer peak increased significantly, which indicates that the formation of the hydrophilic ionic domain was enhanced. A similar tendency was observed in the 50 nm-thick Nafion thin films because the growth of the hydrophilic domain along the in-plane direction was significantly confined as the film thickness approached the domain size.

To further understand the change in the hydrophilic ionic domain, 1D line-integrated analysis results along the in-plane and out-of-plane directions were extracted from the GISAXS 2D images in the same manner as the previous study.³⁸ For the in-plane direction analysis, the distance of the cut line from the beam center was set as $q = 0.45 \text{ nm}^{-1}$ to avoid the influence of the Yoneda peak. For the out-of-plane analysis, the scattering position shift along the q_z direction may have been caused by the refraction of X-ray. The peak shift along the q_z direction was negligibly small, which was confirmed by calculating the d -spacing considering the distorted wave born approximation.³⁸ The typical 1D line profiles along the in-plane direction are displayed in Figure 3. The scattering vector q expressed in reciprocal space can be converted to d -spacing in real space by using following equation:

$$d = \frac{2\pi}{q} \quad (2)$$

The line profiles along the in-plane direction displayed in Figure 3 clearly indicate the differences in the morphologies of these Nafion thin films with different thicknesses and IPA

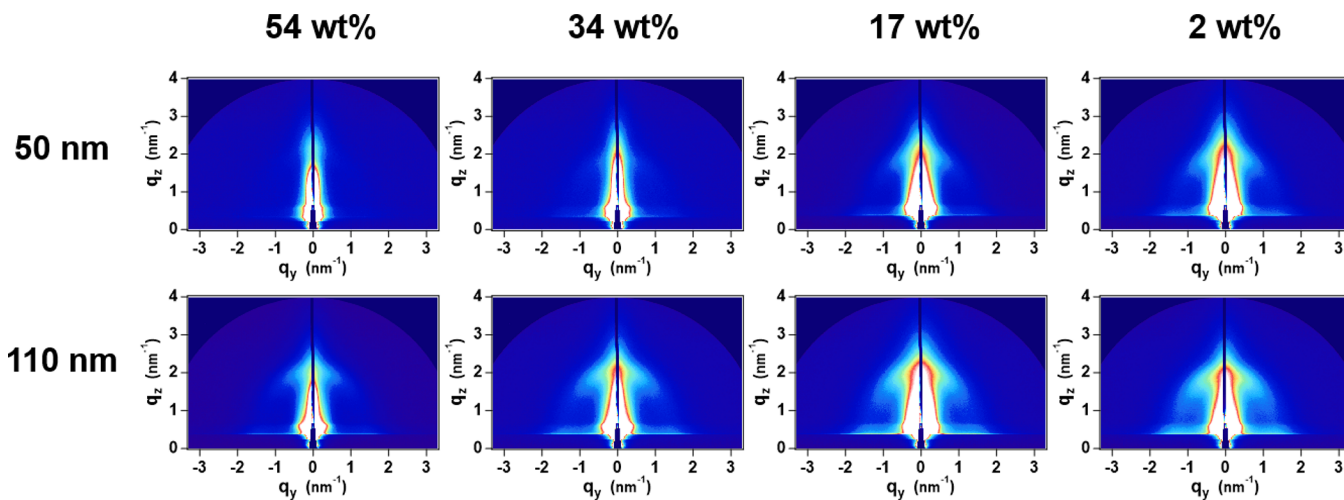


Figure 2. GISAXS 2D patterns of 50 and 110 nm-thick Nafion thin films cast by dispersion with different IPA fractions under 80% RH at 25 °C.

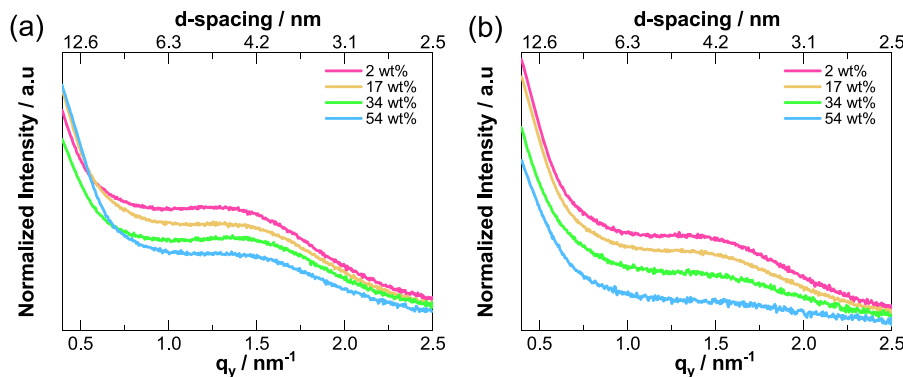


Figure 3. 1D in-plane line profile of Nafion thin films cast by Nafion dispersion with different IPA fractions: (a) 110 nm and (b) 50 nm.

fractions. The intensity of the ionomer peak found in all 50 and 110 nm-thick Nafion thin films increased as the IPA fraction decreased to 2 wt %, and the peak positions marginally shifted to the lower q side to approximately 1.56 and 1.48 nm $^{-1}$, respectively. The hydrophilic ionic peak shown in the line profile (Figure 3) exhibited a similar tendency of proton conductivity, which is also experimentally proved in our previous works.^{38,42} These results indicate that the size of the hydrophilic domain in thin films increased as the IPA fraction of cast dispersion decreased. A similar tendency was observed in the out-of-plane direction (Figure S3).

The Gaussian function was used to fit the ionomer peak to extract the d -spacing of the ionomer peak. Typical fitting results are displayed in Figure S4. The obtained d -spacing versus IPA fraction plot is presented in Figure 4a,b. For 50 and 110 nm-thick Nafion thin films, the d -spacing along the in-plane direction increased to 3.0 and 4.4 nm, respectively, as the IPA fraction decreased to 2 wt %. Although the d -spacing value along the out-of-plane direction indicated in Figure 4b exhibited a similar tendency as displayed in Figure 4a, the out-of-plane value was marginally less than that along the in-plane direction.⁴³ The d -spacing of the cast thin films shown in Figure 3 exhibited a relatively lower value than that of the freestanding Nafion membrane (4.9–5.2 nm) due to the confinement effect in which the growth of the hydrophilic domain of the Nafion thin film was suppressed in this thickness regime.^{38,44} Compared with 110 nm-thick thin films, 50 nm-thick films exhibited lower values because of the significant

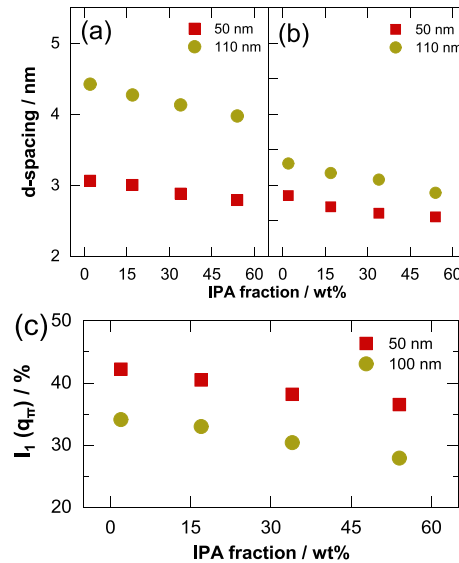


Figure 4. d -Spacing of the ionomer peak extracted from the line profile along (a) in-plane and (b) out-of-plane directions under 80% RH with different IPA fractions. (c) Ratio of contribution of the hydrophilic ionic domain along the out-of-plane component.

confinement effect, which results in the lack of integrity of the domain structure. Overall, the d -spacing decreased monotonically as the IPA fraction of the cast Nafion dispersion increased, which indicates that the alcohol/water ratio in the

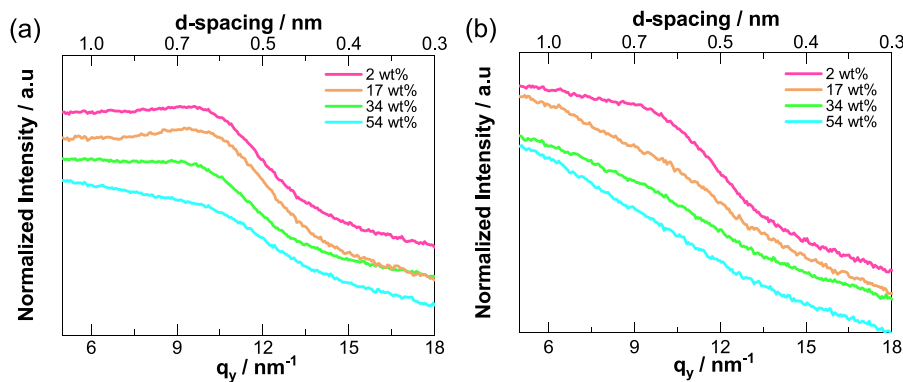


Figure 5. GIWAXS 1D line profile, (a) 110 nm and (b) 50 nm, of the Nafion thin film cast by Nafion dispersion with different IPA fractions extracted from 2D patterns displayed in Figure S6.

Nafion dispersion directly affects the spacing of the hydrophilic ionic domain in cast Nafion thin films. Furthermore, the *d*-spacing along the in-plane direction was greater than that in the out-of-plane direction under the same condition (IPA fraction and thickness), which indicates that the behavior of the hydrophilic domain is anisotropic.

To quantitatively compare the ionomer peak intensity along the meridional axis with that along the equatorial axis, I_1 and I_2 were used, respectively. The curves were normalized by using the same method reported in our previous study.³⁸ Here, we set an assumption that I_1 and I_2 are Gaussian distribution functions of the azimuthal angle, φ , indicated in Figure S5, with peaks along the meridional ($\varphi = 0^\circ$) and equatorial ($\varphi = 90^\circ$) directions. Then, $I_1(\varphi)$ and $I_2(\varphi)$ were utilized to calculate the normalized integral intensity, $I(q)$, which is expressed as the following equation.⁴⁵

$$I_i(q) \approx \int_0^{\pi/2} I_i(\varphi) 2\pi q \sin \varphi d\varphi \quad (3)$$

The meridian and equator scattering patterns refer to the in-plane and out-of-plane directions against the substrate. The calculated normalized integrated intensity of the ionomer peak around $1\text{--}2 \text{ nm}^{-1}$ for the 50 and 110 nm-thick Nafion thin films with different IPA fractions is displayed in Figure 4c. In general, for both 50 and 110 nm-thick films, the contribution of the orientated component along the out-of-plane direction, $I_1(q)$ (%), increased marginally with increasing IPA fraction. This result indicates that the IPA fraction in the casting solution influences the orientation of the nanostructure of the cast film. Considering the absolute intensity of the scattering pattern displayed in Figure 2, it is clear that the film cast by the lower IPA fraction solution is more inclined to be oriented parallel to the Pt substrate than in the case of the film cast by the high IPA fraction solution. A similar result was obtained by Van Cleve *et al.*, who suggested that the film cast with lower IPA fractions induced a more orientated Pt/ionomer interfacial structure owing to the Pt–sulfonate interaction.²⁹

Additionally, GIWAXS measurement was conducted to investigate the molecular aggregation in the hydrophobic domain of the Nafion thin films. The line profiles along the in-plane direction extracted from the GIWAXS images (Figure S6) are displayed in Figure 5. The broad peak observed at around $q = 10\text{--}12 \text{ nm}^{-1}$ can be attributed to the combination of amorphous and crystalline CF_2 chain structures that appeared at $q = 10.5$ and 12 nm^{-1} , respectively.^{34,46} For the 50 nm-thick Nafion thin films displayed in Figure 5b, an

amorphous/crystalline peak was detected in all samples and decreased with increasing IPA fractions, which indicates that the growth of the ordered hydrophobic structure was enhanced as the IPA fraction of the Nafion cast dispersion decreased. Compared with the 50 nm samples, the amorphous/crystalline peak observed at 110 nm (Figure 5a) is comparatively sharp because the bulkier properties begin to dominate the thin-film morphology.³⁵ Similar to the in-plane direction, in the case of the out-of-plane direction, the amorphous/crystalline peak in 110 nm-thick thin films gradually decreased as the IPA fraction increased, which indicates that the lack of integrity of the domain structure is enhanced as the IPA fraction increased (Figure S7a). The 50 nm-thick films exhibited a similar tendency with the 110 nm-thick films (Figure S7b). For further investigation, a crystalline-rich phase proportion, P_c , of the Nafion thin films as reported previously³⁸ was estimated to describe the morphology changes as a function of the IPA fraction. The typical fitting results are displayed in the Supporting Information (Figure S8). As displayed in Figure 6a, the P_c along the in-plane direction generally decreased with an increase in the IPA fraction for a given thickness. In the case

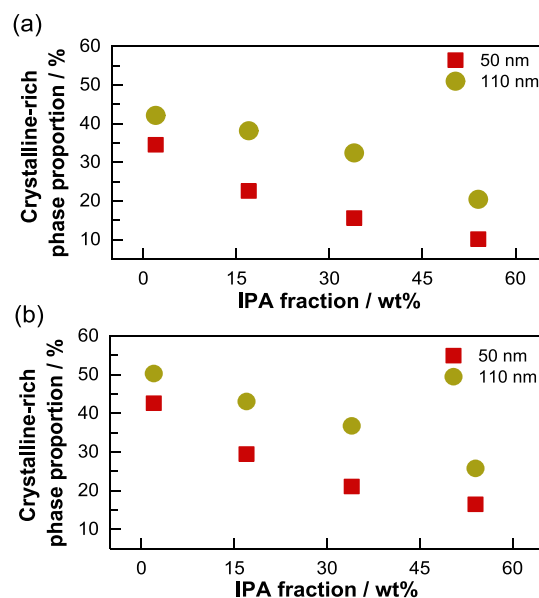


Figure 6. Estimated crystalline-rich phase proportion of Nafion thin films with different IPA fractions along (a) in-plane and (b) out-of-plane directions extracted from GIWAXS 2D patterns.

of the 110 nm-thick Nafion thin films, P_c gradually decreased to 20.4% as the IPA fraction increased to 54 wt %. In the case of the 50 nm-thick Nafion thin films, P_c gradually decreased to 10.1% as the IPA fraction increased to 54 wt %. Compared with the 110 nm films, the 50 nm-thick thin films exhibited a lower P_c owing to the disordered domain structure, as mentioned in the previous section. A similar tendency was observed for P_c in the out-of-plane direction, as indicated in Figure 6b. Moreover, the P_c along the out-of-plane direction exhibited a marginally greater value than the in-plane direction, indicating anisotropic behavior due to the ionomer/substrate interaction. Figure 6 clearly indicates that the crystalline structure of the thin films depends on the IPA fraction of casting solution, thereby implying that the dispersion influences the structural order of the hydrophobic domains in Nafion.

In the following, we discuss the correlation between the IPA fraction and morphology in Nafion thin films. This study indicates that both the morphology and proton conductivity of Nafion thin films are affected by the IPA fraction of the cast dispersion. It has been reported that the morphology of the Nafion molecules in the dispersion changes with the IPA/water ratio.⁴⁷ At low IPA contents, the polar sulfonic groups interact with water, and the nonpolar perfluorocarbon backbones are associated with each other, resulting in a tightly packed structure with the sulfonic group on the outside and the perfluorocarbon backbone inside the Nafion molecules. With increasing IPA content, the nonpolar perfluorocarbon backbones interact with IPA and the polar sulfonic groups associated with each other, resulting in a loosely packed structure with the perfluorocarbon backbone on the outside and the sulfonic group inside the Nafion molecules. Considering the previous study,⁴⁸ in this study, the Nafion molecules in the 2 wt % IPA fraction dispersion have a tightly packed structure with hydrophilic/hydrophobic phase separation because the large amount of water interacts with the sulfonic groups. Conversely, the Nafion molecules in the 54 wt % IPA fraction dispersion have a loosely packed structure with low hydrophilic/hydrophobic phase separation. In the case of the 2 wt % IPA fraction dispersion, the tightly packed structure with a sulfonic group on the outside of the Nafion molecules enhances the development of hydrophilic/hydrophobic phase separation in the Nafion thin film because specific adsorption of Nafion molecules occurs due to the interaction between the sulfonic groups in the Nafion molecules and the surface of the Pt substrate.^{48–50} It has been reported that the morphology of Nafion thin films on substrates is influenced by the interaction between the sulfonic groups and the substrates.^{29,35,42,51,52} In the case of the 54 wt % IPA fraction dispersion, the loosely packed structure of the Nafion molecules with the sulfonic group inside the Nafion molecules inhibits the development of hydrophilic/hydrophobic phase separation in the Nafion thin film. In particular, the effect of the molecular structure on the thin-film morphology is pronounced when the thickness of the Nafion thin film is small as shown in Figure 7. These morphological differences of the Nafion thin films, which are influenced by the Nafion molecular structure in the different IPA fraction dispersions, result in a difference in proton conductivity (Figure 1 and Figure S2). This is because the remarkable confinement effect causes the lack of large backbone bundles with a strong interchain as the thickness is topologically confined to under 50 nm.^{34,44} Our scattering profile indicates that the formation of hydrophilic and

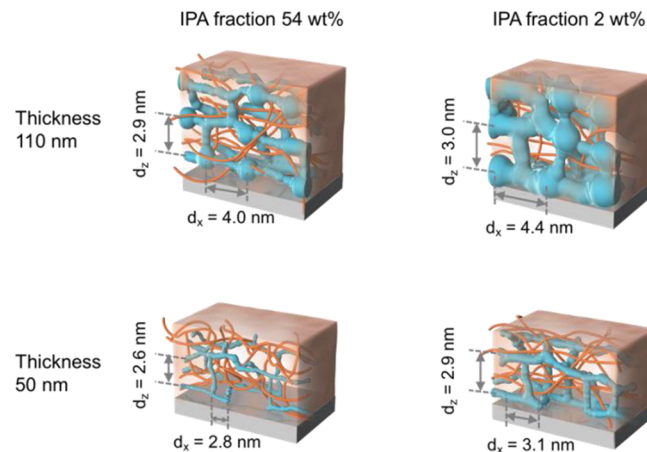


Figure 7. Schematic model of Nafion thin films cast by dispersion with different IPA fractions.

hydrophobic domains are suppressed and not well defined in 50 nm-thick films, which showed dispersion-like properties.³⁵ On the other hand, the confinement effect of 110 nm-thick thin films is relatively not as strong as that of 50 nm-thick thin films, which exhibited membrane-like properties and well-defined hydrophilic/hydrophobic domain structures.^{38,42} As a result, the proton conductivity of cast thin films is more likely to be affected by the water/IPA ratio as the thickness is confined to under 50 nm. The tendency of domain size to vary with IPA or water content is consistent with the previous work conducted by Berlinger *et al.*, who also suggested that the average cluster size increases with increasing water content.³³ In a high-IPA-content solvent, as aforementioned, the Nafion molecules tend to form a tightly packed structure with a highly hydrophilic/hydrophobic phase-separated structure. In this case, it is anticipated that the proton transport pathway is well grown, which is related to comparatively high proton conductivity. Conversely, a low-IPA-content solvent results in a loosely packed structure where the proton transport pathway is restricted owing to the low hydrophilic/hydrophobic phase separation.

CONCLUSIONS

In this study, we systematically investigated the alcohol/water effect in Nafion thin films with thicknesses of 50–110 nm in terms of the morphology and proton transport property via GISAXS/GIWAXS and EIS methods. It is apparent that the water/alcohol ratio in the cast dispersion directly influences the morphology, connectivity of hydrophilic groups, hydrophilic/hydrophobic phase separation, and proton transport behavior in cast films. As the IPA fraction decreased to 2 wt %, the growth of the hydrophilic domain of the cast Nafion thin films is accelerated, accompanied by the formation of a crystalline-rich phase in the hydrophobic domain, which indicates a strong hydrophilic/hydrophobic phase separation. Conversely, Nafion thin films cast with a 54 wt % IPA fraction exhibited the lowest phase separation and proton conductivity value. These results indicate that the morphology of the cast thin films is strongly influenced by the dispersion state in solution. The findings of this study are expected to further understand catalyst/ionomer interfacial phenomena during the optimized dispersion fabrication process in PEFCs.

EXPERIMENTAL SECTION

Sample Preparation. Nafion dispersion was prepared by diluting a 20 wt % Nafion solution in the desired solution, where the solvent compositions were [IPA]/[IPA + water] = 2, 17, 34, and 54 wt % (Nafion weight percent: 18.9, 12.6, 6.8, and 1.1 wt %) by adding ultrapure water. Thereafter, the Nafion thin films were prepared by using the spin-casting method on the interdigitated array electrodes. The thicknesses of the as-prepared Nafion thin films on the interdigitated array electrodes were confirmed by ellipsometry measurements (Otsuka Electronics Co., Ltd.).

Proton Conductivity Measurement. A self-designed Pt-deposited interdigitated array (Osaka Vacuum Industrial Co., Ltd.) with the same setup as in our previous study was used to measure the proton conductivity.³⁸ The proton conductivity of the cast Nafion thin films applied to the interdigitated array electrodes was measured by EIS under a flow of dry N₂ gas through a water tank. The relative humidity in the proton conductivity was changed from 20 to 90% RH at 25 °C. All measurements were conducted at 25 °C with 20–90% relative humidity (RH). The alternating amplitude potential was 100 mV, and the frequency range was between 7 MHz and 0.01 Hz. The collected impedance data were fitted using analysis software EC-lab to calculate the Nation thin-film resistances. For the pre-experiment, the proton conductivity of the 200 nm thin film was measured at 15 min time intervals under 80% RH at 25 °C, which shows that there is almost no obvious change in the Nyquist plot after 60 min (Figure S1f). Therefore, both maintained electrochemical impedance and GISAXS/GIWAXS measurements more than 60 min before measurement.

GISAXS/GIWAXS Measurements. For GISAXS/GIWAXS measurements, Nafion thin films with thicknesses of 50 and 110 nm were prepared on a Pt-sputtered Si substrate as previously reported.³⁸ The sample was placed into a self-designed environmental chamber, in which humidity was controlled. The relative humidity was controlled to a constant humidity level (80% RH at 25 °C). All GISAXS and GIWAXS measurements were conducted in beamline BL40B2 at SPring-8, Hyogo, Japan. The incident X-ray energy and angle were set at 12.4 keV and 0.14°, respectively. The detectors for the GISAXS and GIWAXS 2D images were a Dectris Pilatus imaging plate (0.172 mm × 0.172 mm, C9729DK-10) and a flat panel sensor (0.05 mm, Hamamatsu Photonics K.K. Japan), respectively. Sample-to-detector distances were approximately 2200 and 60 mm for the GISAXS and GIWAXS configurations, respectively. To calibrate the beam center and sample-to-detector distance for GISAXS and GIWAXS, silver behenate and CeO₂ were used as standard materials, respectively. Considering the influence of water molecules on collected scattering profiles, we estimated the electron density (ρ_e) of water and the Nafion molecule (EW = 1100) based on following equation:

$$\rho_e = \rho \left(\frac{N_A}{A} \right) Z \quad (4)$$

N_A represents Avogadro's constant, A is the molecular weight, and Z is the number of electrons per molecule. We used the equivalent weight (EW = 1100) of Nafion as the molecular weight and calculated the number m of CF₂CF₂, from the equation EW = 100m + 446.⁸ It has been reported that the densities of Nafion under dry and wet conditions are approximately 2.08 and 1.86 g/cm³, respectively.⁵³ As the

estimated electron densities of Nafion under dry and wet conditions are 0.609 and 0.522 e/Å³, which are much larger than that of the water molecule (0.334 e/Å³), the effect of water is almost negligible.

ASSOCIATED CONTENT

Supporting Information

The Supporting Information is available free of charge at <https://pubs.acs.org/doi/10.1021/acsomegaf00607>.

Nyquist plot of Nafion thin films and the equivalent circuit used for extracting film resistance; enlarged proton conductivity of Nafion thin films; 1D out-of-plane line profiles of Nafion thin films cast by Nafion dispersion with various IPA fractions extracted; typical Gaussian fitting result of the 1D line profile of GISAXS patterns in the Nafion thin film; typical normalized azimuthal plot of GISAXS patterns in the Nafion thin film; GIWAXS 2D patterns of the Nafion thin film cast by dispersion with various IPA fractions; 1D out-of-plane GIWAXS line profiles of Nafion thin films cast by Nafion dispersion with various IPA fractions extracted; typical normalized azimuthal plot of GIWAXS patterns in the Nafion thin film (PDF)

AUTHOR INFORMATION

Corresponding Author

Kentaro Yamamoto — Graduate School of Human and Environmental Studies, Kyoto University, Kyoto 606-8316, Japan;  orcid.org/0000-0002-8739-4246; Email: yamamoto.kentaro.4e@kyoto-u.ac.jp

Authors

Xiao Gao — Graduate School of Human and Environmental Studies, Kyoto University, Kyoto 606-8316, Japan; Present Address: Present address: The School of Chemical Engineering, Nanjing University of Science and Technology, XuanWu District, Nanjing 210-094, China (X.G.);  orcid.org/0000-0002-5469-1754

Tomoyasu Hirai — Department of Applied Chemistry, Osaka Institute of Technology, Osaka 535-8585, Japan;  orcid.org/0000-0002-6441-5163

Noboru Ohta — Japan Synchrotron Radiation Research Institute (JASRI), Sayo-gun, Hyogo 679-5198, Japan

Tomoki Uchiyama — Graduate School of Human and Environmental Studies, Kyoto University, Kyoto 606-8316, Japan;  orcid.org/0000-0003-4880-7498

Toshiki Watanabe — Graduate School of Human and Environmental Studies, Kyoto University, Kyoto 606-8316, Japan;  orcid.org/0000-0003-1798-1987

Hideto Imai — Nissan Analysis and Research Center, Yokosuka-shi, Kanagawa 237-8523, Japan;  orcid.org/0000-0002-9434-1492

Seiho Sugawara — Fuel Cell Cutting-Edge Research Center Technology Research Association, Tokyo 135-0064, Japan; Present Address: Present address: Nissan Motor Co., Ltd., 1, Natsushima-cho, Yokosuka-shi, Kanagawa 237-8523, Japan (S.S.).

Kazuhiko Shinohara — Fuel Cell Cutting-Edge Research Center Technology Research Association, Tokyo 135-0064, Japan

Yoshiharu Uchimoto — Graduate School of Human and Environmental Studies, Kyoto University, Kyoto 606-8316, Japan; orcid.org/0000-0002-1491-2647

Complete contact information is available at:
<https://pubs.acs.org/10.1021/acsomega.1c00607>

Notes

The authors declare no competing financial interest.

ACKNOWLEDGMENTS

This research is based on results obtained from a project commissioned by the New Energy and Industrial Technology Development Organization (NEDO). This study was partially supported by the synchrotron radiation experiments performed at BL40B2 of SPring-8 with the approval of the Japan Synchrotron Radiation Research Institute (JASRI) (proposal numbers 2018A1020, 2018B1034, 2019A1025, 2019B1023, and 2019B1024).

REFERENCES

- (1) Eikerling, M.; Kulikovsky, A. *Polymer Electrolyte Fuel Cells: Physical Principles of Materials and Operation*; CRC Press, 2014.
- (2) Franco, A. A. *Polymer Electrolyte Fuel Cells: Science, Applications, and Challenges*; Pan Stanford Publishing, 2016.
- (3) Kreuer, K. D. *Fuel Cells: Selected Entries from the Encyclopedia of Sustainability Science and Technology*; Springer: New York, 2012.
- (4) Li, H.; Knights, S.; Shi, Z.; Van Zee, J. W.; Zhang, J. *Proton Exchange Membrane Fuel Cells: Contamination and Mitigation Strategies*; CRC Press, 2010.
- (5) Kreuer, K.-D.; Paddison, S. J.; Spohr, E.; Schuster, M. Transport in Proton Conductors for Fuel-Cell Applications: Simulations, Elementary Reactions, and Phenomenology. *Chem. Rev.* **2004**, *104*, 4637.
- (6) Divoux, G. M.; Finlay, K. A.; Park, J. K.; Song, J.-M.; Yan, B.; Zhang, M.; Dillard, D. A.; Moore, R. B. Morphological Factors Affecting the Behavior of Water in Proton Exchange Membrane Materials. *ECS Trans.* **2011**, *41*, 87.
- (7) Kusoglu, A.; Weber, A. Z. New Insights into Perfluorinated Sulfonic-Acid Ionomers. *Chem. Rev.* **2017**, *117*, 987.
- (8) Mauritz, K. A.; Moore, R. B. State of Understanding of Nafion. *Chem. Rev.* **2004**, *104*, 4535.
- (9) Rodgers, M. P.; Bonville, L. J.; Kunz, H. R.; Slattery, D. K.; Fenton, J. M. Fuel cell perfluorinated sulfonic acid membrane degradation correlating accelerated stress testing and lifetime. *Chem. Rev.* **2012**, *112*, 6075.
- (10) Zhang, H.; Shen, P. K. Recent Development of Polymer Electrolyte Membranes for Fuel Cells. *Chem. Rev.* **2012**, *112*, 2780.
- (11) Holdcroft, S. Fuel Cell Catalyst Layers: A Polymer Science Perspective. *Chem. Mater.* **2014**, *26*, 381.
- (12) Weber, A. Z.; Borup, R. L.; Darling, R. M.; Das, P. K.; Dursch, T. J.; Gu, W.; Harvey, D.; Kusoglu, A.; Litster, S.; Mench, M. M.; et al. A Critical Review of Modeling Transport Phenomena in Polymer-Electrolyte Fuel Cells. *J. Electrochem. Soc.* **2014**, *161*, F1254.
- (13) Paul, D. K.; McCreery, R.; Karan, K. Proton Transport Property in Supported Nafion Nanothin Films by Electrochemical Impedance Spectroscopy. *J. Electrochem. Soc.* **2014**, *161*, F1395.
- (14) Paul, D. K.; Shim, H. K. K.; Giorgi, J. B.; Karan, K. Thickness dependence of thermally induced changes in surface and bulk properties of Nafion nanofilms. *J. Polym. Sci., Part B: Polym. Phys.* **2016**, *54*, 1267.
- (15) Jinnouchi, R.; Kudo, K.; Kitano, N.; Morimoto, Y. Molecular Dynamics Simulations on O₂ Permeation through Nafion Ionomer on Platinum Surface. *Electrochim. Acta* **2016**, *188*, 767.
- (16) Siroma, Z.; Kakitsubo, R.; Fujiwara, N.; Ioroi, T.; Yamazaki, S.-i.; Yasuda, K. Depression of proton conductivity in recast Nafion film measured on flat substrate. *J. Power Sources* **2009**, *189*, 994.
- (17) Tesfaye, M.; Kushner, D. I.; Kusoglu, A. Interplay between Swelling Kinetics and Nanostructure in Perfluorosulfonic Acid Thin-Films: Role of Hygrothermal Aging. *ACS Appl. Polymer Mater.* **2019**, *1*, 631.
- (18) Kushner, D. I.; Kusoglu, A.; Podraza, N. J.; Hickner, M. A. Substrate-Dependent Molecular and Nanostructural Orientation of Nafion Thin Films. *Adv. Funct. Mater.* **2019**, *29*, 1902699.
- (19) Aldebert, P.; Dreyfus, B.; Pineri, M. Small-angle neutron scattering of perfluorosulfonated ionomers in solution. *Macromolecules* **1986**, *19*, 2651.
- (20) Aldebert, P.; Gebel, G.; Loppinet, B.; Nakamura, N. Polyelectrolyte effect in perfluorosulfonated ionomer solutions. *Polymer* **1995**, *36*, 431.
- (21) Loppinet, B.; Gebel, G.; Williams, C. E. Small-Angle Scattering Study of Perfluorosulfonated Ionomer Solutions. *J. Phys. Chem. B* **1997**, *101*, 1884.
- (22) Szajdzinska-Pietek, E.; Schlick, S.; Plonka, A. Self-Assembling of Perfluorinated Polymeric Surfactants in Water. Electron-Spin Resonance Spectra of Nitroxide Spin Probes in Nafion Solutions and Swollen Membranes. *Langmuir* **1994**, *10*, 1101.
- (23) Szajdzinska-Pietek, E.; Schlick, S.; Plonka, A. Self-assembling of perfluorinated polymeric surfactants in nonaqueous solvents. Electron spin resonance spectra of nitroxide spin probes in Nafion solutions and swollen membranes. *Langmuir* **1994**, *10*, 2188.
- (24) Li, H.; Schlick, S. Effect of solvents on phase separation in perfluorinated ionomers, from electron spin resonance of VO₂⁺ in swollen membranes and solutions. *Polymer* **1995**, *36*, 1141.
- (25) Lin, H. L.; Yu, T. L.; Huang, C. H.; Lin, T. L. Morphology study of Nafion membranes prepared by solutions casting. *J. Polym. Sci., Part B: Polym. Phys.* **2005**, *43*, 3044.
- (26) Ma, C.-H.; Yu, T. L.; Lin, H.-L.; Huang, Y.-T.; Chen, Y.-L.; Jeng, U.-S.; Lai, Y.-H.; Sun, Y.-S. Morphology and properties of Nafion membranes prepared by solution casting. *Polymer* **2009**, *50*, 1764.
- (27) Tarokh, A.; Karan, K.; Ponnurangam, S. Atomistic MD Study of Nafion Dispersions: Role of Solvent and Counterion in the Aggregate Structure, Ionic Clustering, and Acid Dissociation. *Macromolecules* **2019**, *53*, 288–301.
- (28) Ngo, T. T.; Yu, T. L.; Lin, H.-L. Influence of the composition of isopropyl alcohol/water mixture solvents in catalyst ink solutions on proton exchange membrane fuel cell performance. *J. Power Sources* **2013**, *225*, 293.
- (29) Van Cleve, T.; Khandavalli, S.; Chowdhury, A.; Medina, S.; Pylypenko, S.; Wang, M.; More, K. L.; Kariuki, N.; Myers, D. J.; Weber, A. Z. Dictating Pt-Based Electrocatalyst Performance in Polymer Electrolyte Fuel Cells, from Formulation to Application. *ACS Appl. Mater. Interfaces* **2019**, *11*, 46953.
- (30) Li, S.; Terao, K.; Sato, T. Colloidal Dispersion of a Perfluorosulfonated Ionomer in Water–Methanol Mixtures. *Polymer* **2018**, *10*, 72.
- (31) Yang, F.; Xin, L.; Uzunoglu, A.; Qiu, Y.; Stanciu, L.; Ilavsky, J.; Li, W.; Xie, J. Investigation of the interaction between nafion ionomer and surface functionalized carbon black using both ultrasmall angle X-ray scattering and Cryo-TEM. *ACS Appl. Mater. Interfaces* **2017**, *9*, 6530.
- (32) Takahashi, S.; Shimanuki, J.; Mashio, T.; Ohma, A.; Tohma, H.; Ishihara, A.; Ito, Y.; Nishino, Y.; Miyazawa, A. Observation of ionomer in catalyst ink of polymer electrolyte fuel cell using cryogenic transmission electron microscopy. *Electrochim. Acta* **2017**, *224*, 178.
- (33) Berlinger, S. A.; McCloskey, B. D.; Weber, A. Z. Inherent acidity of perfluorosulfonic acid ionomer dispersions and implications for ink aggregation. *J. Phys. Chem. B* **2018**, *122*, 7790.
- (34) Kusoglu, A.; Dursch, T. J.; Weber, A. Z. Nanostructure/Swelling Relationships of Bulk and Thin-Film PFSA Ionomers. *Adv. Funct. Mater.* **2016**, *26*, 4961.
- (35) Kusoglu, A.; Kushner, D.; Paul, D. K.; Karan, K.; Hickner, M. A.; Weber, A. Z. Impact of Substrate and Processing on Confinement of Nafion Thin Films. *Adv. Funct. Mater.* **2014**, *24*, 4763.

- (36) Tesfaye, M.; MacDonald, A. N.; Dudenas, P. J.; Kusoglu, A.; Weber, A. Z. Exploring substrate/ionomer interaction under oxidizing and reducing environments. *Electrochim. Commun.* **2018**, *87*, 86.
- (37) Dudenas, P. J.; Kusoglu, A. Evolution of Ionomer Morphology from Dispersion to Film: An in Situ X-ray Study. *Macromolecules* **2019**, *52*, 7779.
- (38) Gao, X.; Yamamoto, K.; Hirai, T.; Uchiyama, T.; Ohta, N.; Takao, N.; Matsumoto, M.; Imai, H.; Sugawara, S.; Shinohara, K. Morphology Changes in Perfluorosulfonated Ionomer from Thickness and Thermal Treatment Conditions. *Langmuir* **2020**, *36*, 3871.
- (39) Saito, I.; Miyazaki, T.; Yamamoto, K. Depth-resolved structure analysis of cylindrical microdomain in block copolymer thin film by grazing-incidence small-angle x-ray scattering utilizing low-energy x-rays. *Macromolecules* **2015**, *48*, 8190.
- (40) Bass, M.; Berman, A.; Singh, A.; Konovalov, O.; Freger, V. Surface Structure of Nafion in Vapor and Liquid. *J. Phys. Chem. B* **2010**, *114*, 3784.
- (41) Bass, M.; Berman, A.; Singh, A.; Konovalov, O.; Freger, V. Surface-Induced Micelle Orientation in Nafion Films. *Macromolecules* **2011**, *44*, 2893.
- (42) Gao, X.; Yamamoto, K.; Hirai, T.; Ohta, N.; Uchiyama, T.; Watanabe, T.; Takahashi, M.; Takao, N.; Imai, H.; Sugawara, S. Substrate-dependent proton transport and nanostructural orientation of perfluorosulfonic acid polymer thin films on Pt and carbon substrate. *Solid State Ionics* **2020**, *357*, 115456.
- (43) Shi, S.; Dursch, T. J.; Borup, R. L.; Weber, A. Z.; Kusoglu, A. Effect of Hygrothermal Ageing on PFSA Ionomers' Structure/Property Relationship. *ECS Trans.* **2015**, *69*, 1017.
- (44) Modestino, M. A.; Paul, D. K.; Dishari, S.; Petrina, S. A.; Allen, F. I.; Hickner, M. A.; Karan, K.; Segalman, R. A.; Weber, A. Z. Self-Assembly and Transport Limitations in Confined Nafion Films. *Macromolecules* **2013**, *46*, 867.
- (45) Kido, M.; Nojima, S.; Ishige, R.; White, K. L.; Kamitani, K.; Ohta, N.; Hirai, T.; Takahara, A. Effect of molecular weight on microcrystalline structure formation in polymer with perylenediimide side chain. *J. Polym. Sci., Part B: Polym. Phys.* **2016**, *54*, 2275.
- (46) Kusoglu, A.; Modestino, M. A.; Hexemer, A.; Segalman, R. A.; Weber, A. Z. Subsecond Morphological Changes in Nafion during Water Uptake Detected by Small-Angle X-ray Scattering. *ACS Macro Lett.* **2011**, *1*, 33.
- (47) Karan, K. Interesting Facets of Surface, Interfacial, and Bulk Characteristics of Perfluorinated Ionomer Films. *Langmuir* **2019**, *35*, 13489.
- (48) Yagi, I.; Inokuma, K.; Kimijima, K. i.; Notsu, H. Molecular Structure of Buried Perfluorosulfonated Ionomer/Pt Interface Probed by Vibrational Sum Frequency Generation Spectroscopy. *J. Phys. Chem. C* **2014**, *118*, 26182.
- (49) Chlistunoff, J.; Pivovar, B. Effects of Ionomer Morphology on Oxygen Reduction on Pt. *J. Electrochem. Soc.* **2015**, *162*, F890.
- (50) Kodama, K.; Jinnouchi, R.; Suzuki, T.; Murata, H.; Hatanaka, T.; Morimoto, Y. Increase in adsorptivity of sulfonate anions on Pt (111) surface with drying of ionomer. *Electrochim. Commun.* **2013**, *36*, 26.
- (51) Paul, D. K.; Karan, K.; Docolis, A.; Giorgi, J. B.; Pearce, J. Characteristics of Self-Assembled Ultrathin Nafion Films. *Macromolecules* **2013**, *46*, 3461.
- (52) Paul, D. K.; Fraser, A.; Karan, K. Towards the understanding of proton conduction mechanism in PEMFC catalyst layer: Conductivity of adsorbed Nafion films. *Electrochim. Commun.* **2011**, *13*, 774.
- (53) Takamatsu, T.; Eisenberg, A. Densities and expansion coefficients of nafion polymers. *Jpn. J. Appl. Phys.* **1979**, *24*, 2221.